Characterization of Fiber Optics Devices for LASIC II

Morgan Dixon
Department of Physics and Astronomy, Carleton College, Northfield, Minnesota

Abstract

Interferometers used for gravitational wave detection require highly stabilized lasers in order to detect small changes in arm lengths. LASIC II uses a hyperfine transition of Iodine to stabilize a Nd:YAG laser to be used aboard LISA. Two fiber optics devices important to the experiment are an Evanescent Optics evanescent wave coupler (EWC) and a Jenoptik electro-optic phase modulator (EOM). It was determined that both are polarizing maintaining, following manufacturer specifications. The EWC has a mechanical hysteresis altering the location of maximum evanescent wave output, which the manufacturer warns of. The input beam to the EOM must be of the correct polarization to obtain expected insertion losses and its characteristic V_π is found to vary with the frequency of modulation, however, the exact relationship between the two quantities is unknown.

1. Introduction

Contrary to Newton describing gravity as an "action at a distance" force, Albert Einstein's Theory of General Relativity imposes a speed limit on gravity, a consequence of which is gravitational waves [1]. Described as ripples in spacetime, gravitational radiation applies stretching and compressing tidal forces upon matter without significantly altering the gravitational wave. Since gravitational waves propagate nearly unaltered through space time they contain undisturbed sources of information about their creation, whether it be astrophysical or cosmological in origin. Observing gravitational waves would lead to unprecedented knowledge of the astrophysical bodies which emit them, such as rotating binary neutron stars and binary black holes, as well as the time period, $t \approx t_{dec}$, after the big bang when gravitons, the force carrier particle of gravity, broke free from the primordial plasma, providing information about physics at high energies as of yet experimentally obtained on Earth [2].

Gravitational waves were first indirectly detected by Joseph Taylor and Russel Hulse, who observed the expected effects of gravitational radiation on a pulsar in a binary orbit with a neutron star. Attempts have been made to directly observe gravitational waves since the 1960's, when Joseph Weber first introduced what are now known as Weber Bars, long aluminum bars constructed to resonate at the expected frequency of passing gravitational waves. While Weber failed to directly observe gravitational waves, current experiments hope to observe slight changes in interferometer arm lengths due to gravitational wave tidal forces. Two land based projects include LIGO and VIRGO, however, they are limited by seismic noise, so LISA, an interferometer set to operate in space, is in planning [1]. In order to make precise measurements of the interferometer arm lengths and determine if a variation is due to a gravitational wave, very stable lasers are necessary. One method of stabilizing lasers is through a hyperfine transition of iodine, as the LASIC project has achieved and the LASIC II project is hoping to improve upon and make space worthy for LISA [3].

One goal of LASIC II is to decrease the size of the stabilization apparatus, which can be achieved by using fiber optics to guide laser beams as opposed to free beams. Two fiber optics devices to be used in the proposed LASIC II apparatus are an Evanescent Wave Coupler and an Electro-Optic Modulator. Before these devices are used in the apparatus, it is important to know whether they work according to the manufacturer's specifications, which was the goal of the experiments presented in this paper. First the polarization of the devices was studied, namely determining if the devices were polarizing maintaining, that is, if a linearly polarized beam is input into the device the output beam is also linearly polarized. Specific to the Evanescent Wave Coupler, the coupling ra-

tio of how the device splits an input laser beam was studied. Finally, the characteristic V_π of the Electro-Optic Modulator was studied to find how it changes with the frequency at which the device is modulated.

It was found that both the Evanescent Wave Coupler and Electro-Optic Modulator are indeed polarizing maintaining, following manufacturer specifications. Additionally, a non-fibered Acousto-Optic Modulator was found to be polarizing maintaining, which was necessary for the apparatus to study the Electro-Optic Modulator. The coupling ratio of the Evanescent Wave Coupler varied as expected, where a mechanical hysteresis altering the location of the maximum evanescent wave power output makes the device more difficult to use, however, the manufacturer warns of this complication. Finally, it was found that the characteristic V_π changes with the modulation frequency of the Elector-Optic Modulator, however, the exact relationship between the two quantities is as of yet unknown. Unexpectedly high values of V_π were found, some surpassing 5 V, complicating the final results, as the manufacturer specifies that at a modulation frequency of 1 kHz V_π = 3.2V, which does not match experimental results and no mention is made that V_π could depend on the frequency of modulation.

2. Background

2.1 Gravitational Waves

Gravity and it's effects have fascinated human kind since antiquity. Greek philosophers, such as Plato and his student Eudoxus, described the motion of heavenly bodies in terms of a series of perfect crystal sphere centered on the Earth, which was updated by Ptolemy in Alexandria, who added the "primum mobile" or the primary mover as the motivating force behind the movement of the stars. The Ptolemic model was criticized by Islamic scholars but it was not until Copernicus revised the Greek philosopher Aristoxenus' work and reintroduced a heliocentric model of the solar system and Kepler introduced elliptical orbits as opposed to circular orbits, that the correct model of planetary motion was constructed [4]. Galileo then discovered the constant of acceleration due to gravity and supported the Copernican model of the solar system. Newton followed with three fundamental laws of motion and a mathematical formalism of gravity's effects that successfully predicted Kepler's laws of planetary motion, the universal law of gravitation. One important consequence of Newton's gravity which "acts at a distance" is that the force propagates at an infinite speed. In the case of a rapidly changing gravitational field, for example, with rotating binary neutron stars, the field would instantaneously change and an observer could register those changes immediately. With no time delay there could be no gravitational waves as the gravitational energy does not need to propagate. The idea of gravity acting at a distance was disquieting to some physicists, amongst whom was Laplace. Laplace attempted to resolve the problem by describing gravity as a fluid which moved from its source to the body it affected at a finite speed, however, he was unable to observe the expected effects of gravity moving at a finite speed, thus he concluded that the speed of gravity must be large, in fact, larger than the speed of light. Laplace had the correct idea, however, once Einstein introduced the Theory of Special Relativity [5] in 1905, the universal speed limit of c, the speed of light, was imposed, ruling out the possibility that gravity could move faster than the speed of light. Then, in 1916 Einstein published the Theory of General Relativity [6], which gives the finite speed of c to gravity, consequently introducing the possibility of gravitational waves, which were later mathematically formalized by teams of physicists in the 1960's and 1970's [1].

Deriving from two main sources, cosmological origins and astrophysical bodies, gravitational radiation is expected to be observed as a superposition of the many sources of gravitational waves, called the stochastic gravitational wave background (SGWB) [7], where each source emits gravitational radiation at unique frequencies. Two types of waves are longitudinal and transverse waves, differing in their direction of propagation. Longitudinal waves, such as sound

waves, propagate in the direction of motion, whereas transverse waves propagate in the plane perpendicular to that of the direction of motion, and include water waves, electromagnetic waves as well as gravitational waves. However, different from water waves and electromagnetic waves, which propagate through water and by oscillating electromagnetic fields respectively, gravitational waves propagate through space-time, the four dimensional "fabric" consisting of the familiar three dimensions of space where time is the fourth dimension [1]. How a gravitational wave propagates through space-time can be imagined as follows. A mass distorts the space-time in which it exists analogous to the distortion created by a tennis ball placed on a taut fabric. Once the ball is stationary the fabric too is stationary. Even if the ball were spinning within the divot it created in the fabric, the fabric would not be moving [8]. This is similar to how a rotating astrophysical body will not create gravitational radiation whereas a body with a changing gravitational field, such as a star collapsing in a supernova or a binary system of neutron stars or black holes, creates gravitational radiation which can be observed as gravitational waves [1]. The cosmological source of gravitational waves comes from the moments after the big bang when the universe was a high energy plasma of particles, and gravitons, the force carrier particle of gravity, were able to break from the high energy plasma and radiate through space-time [2].

We come to observe gravitational waves as they propagate through space-time to Earth, similar to replacing the taut fabric from above with a still pool of water, where the disturbance of the tennis ball creates waves which propagate out from the point of contact. As the water waves move away from the point of origin their amplitude decreases, which also occurs with gravitational waves, whose amplitude decreases inversely with the distance traveled, $\frac{1}{r}$, where r is the distance traveled, as shown in Figure 1 [9]. This means that gravitational waves traveling long distances diminish in amplitude and are weak by the time they reach Earth. While gravitational wave signals are weak, one of their important properties is that they distort mass they may encounter as they travel but do not significantly loose energy, meaning that the information they contain is not appreciably changed from their creation to their observation, making them a critical tool to further study their sources [10].

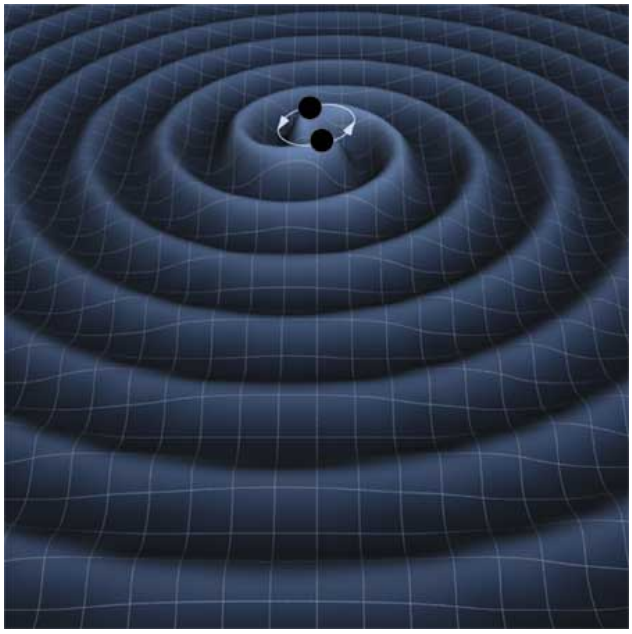

Figure 1: In this artists rendition of a gravitational wave the gridded two dimensional surface represents the truly four dimensional space-time, where the two black holes in a binary orbit create the disturbance in space-time which propagates away from the origin in waves of decreasing amplitude.

For example, they provide direct access to the mass and period of rotation of rotating neutron stars and even allow for detection of pulsars that have not been found by radio detection. Detection of gravitational waves will also further the study of black holes as the only information that they directly emit is gravitational radiation and nearly undetectable Hawkings radiation, improving upon the current indirect methods of observing black holes by the effects they impose upon their surroundings [1]. Background gravitational radiation will also provide cosmological information about the inflationary models, pre-Big-Bang models, electroweak phase transition, and cosmic strings, allowing physicists to probe the earliest states of the universe, for example, when it was

less than one minute old, a feat as of yet not accomplished experimentally [7] as the energy at that time was higher than we are currently capable of creating on Earth.

2.2 Detection of Gravitational Waves

Gravitational wave detection involves observing how an incoming gravitational waves distorts a mass, for example as shown in Figure 2 [1], where a gravitational wave distorts a circle of free particles by changing the circle to an ellipse of the same area, corresponding to tidal stretching and compressing of a solid mass, detectable by changes in length. However the change in distance of a test particle due to a gravitational wave is predicted to be at largest, 10^{-18} m, which is smaller than the diameter of a proton and the thermal motion of atoms in a test mass [1].

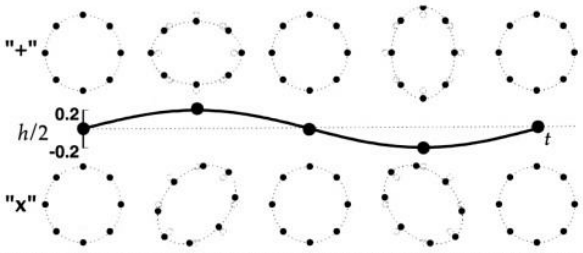

Figure 2: Each ring of dots represents a ring of free particles, where the top and the bottom lines of rings are distorted into different ellipses as a gravitational wave passes but are identical, perfect circles, when there is no gravitational wave or it is equidistant from the masses.

In the 1960's Joseph Weber was the first physicist to attempt to observe gravitational waves using an apparatus now known as Weber Bars. The original bar was two meters long and constructed from aluminum with piezoelectric sensors attached to convert vibrations to electric signals. The bar was constructed such that a gravitational wave traveling at a right angle to the long axis of the bar would stretch and compress the bar along this axis, and if vibrated at the correct frequency, 1 kHz, determined by the expected frequency of gravitational waves emitted from astrophysical sources such as coalescing binary neutron stars, the bar would amplify the vibrations to ease detection. By placing one bar in Maryland and a twin at Argonne National Laboratory, Weber was able to cancel seismic noise and random thermal noise unique to each bar and observe the signals common between the two, believed to be gravitational waves. However, repetitions of his experiment elsewhere produced not but the expected noise, providing inconclusive results as to Weber's observations and leaving the scientific community without a direct observation of gravitational waves. While Weber was unable to obtain conclusive results, some current experiments continue to use Weber Bars, however, cooled to a temperature of 0.1 K to reduce thermal noise [1].

While Weber failed to prove the existence of gravitational waves, Joseph Taylor and Russel Hulse in 1974 observed gravitational waves indirectly by their effects on a binary pulsar. Hulse observed a pulsar with a variable pulsation period, the first of it's kind, and it was determined with Taylor that the pulsar is in a binary orbit with a neutron star, moving at highly relativistic speeds of nearly 0.1% the speed of light in an elliptical orbit. These qualities allowed the pair to observe a gravitational redshift in the change of spin rate as the pulsar moved through it's orbit as well as the orbit shrinking as the gravitational radiation carries energy away from the system, two effects predicted by the existence of gravitational radiation and providing an indirect detection of gravitational waves [1].

Even though Taylor and Hulse have proved the existence of gravitational waves it is desirable to directly observe the radiation in order to study it's source, leading physicists to the current gravitational wave detectors which use interferometers.

2.3 Interferometers

The basic principle of an interferometer is to split a light source into two or more partial beams then send each beam on a different path and recombine the partial beams to create an interference pattern which changes depending upon the difference in path lengths and or phases. Using the effects of interferometry it is possible to determine the path length difference between the

split beams, the basic premise of gravitational wave detectors, as a gravitational wave's tidal effects would cause stretching and compression of the two paths. Two basic interferometers, the Michaelson, the Mach-Zhender Interferometers, as well as a Fabry-Perot Cavity, also called a Fabry-Perot Interferometer, are described below.

Created by Albert Michaelson, the Michaelson Interferometer uses a beam splitter to split a monochromatic beam into two parts of equal intensities, where a two plane mirrors redirect each beam back to the beam splitter and the interfered beams are incident upon a detector, as shown in Figure 3. One advantage of this interferometer is that when the arms are of equal length the noise and instabilities originating from the laser are canceled as the two interfered beams. This configuration also allows for easy distance measurements since moving one mirror a distance equal to a mere quarter of a wavelength of the light in the apparatus, $\frac{\lambda}{4}$, produces a change in the interference pattern at the detector from constructive to destructive interference [11].

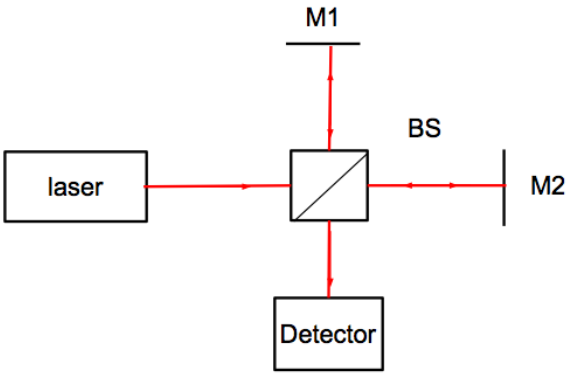

Figure 3: The basic apparatus for a Michaelson Interferometer. A monochromatic light source is split by a beam splitter, BS, then each beam is reflected back towards the BS by means of two plane mirrors, M1 and M2, where the beams are recombined into one and sent to a detector, which detects the interference pattern created by a change in arm length.

A modified version of the Michaelson Interferometer, a Mach-Zhender Interferometer, allows for precise measurements of phase shift between the split beams, a basic apparatus for which is shown in Figure 4. Beginning similarly to a Michaelson Interferometer, a Mach-Zhender Interferometer splits a monochromatic light source with a beam splitter, sending each beam on a separate path guided by a plane mirror. Instead of recombining the two beams by the same beam splitter that split them, they are recombined by a second beam splitter and the interfered beam is sent to a detector. Reflections off of the plane mirrors introduce phase shifts and are different for the two beams as the beam splitter introduces different phase shifts for the beams that are reflected and transmitted through the cube [12].

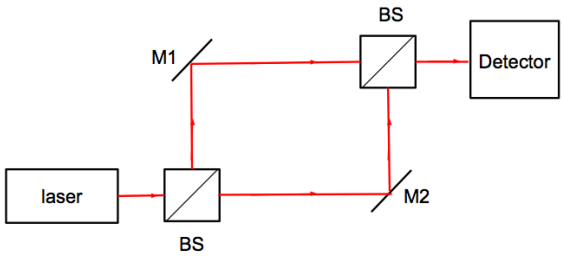

Figure 4: A Mach-Zhender Interferometer begins with a monochromatic light source which is split by a beam splitter, BS, where the two beams are directed by two plane mirrors, M1 and M2, to a second beam splitter which recombines the two beams and transmits the recombined beam to be detected.

A Fabry-Perot Cavity or Interferometer consists of two mirrors facing one another, either plane or spherical mirrors of equal radii, where the mirrors are positioned such that a beam incident parallel to the axis of the interferometer resonates within the cavity. A spherical cavity is shown in Figure 5 [12]. Such cavities are useful as they resonate most efficiently when the frequency of the laser is an integer multiple of the quantity, $\frac{c}{2L}$, where L is the length of the cavity, and the maximum transmission occurs at the same frequencies, creating a filter on the frequency of the laser, narrowing it's bandwidth [10].

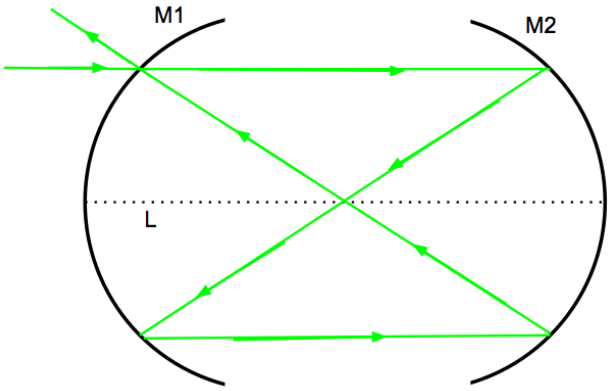

Figure 5: A spherical Fabry-Perot Cavity consists of two spherical mirrors of equal radii, M1 and M2, aligned along the axis, shown in a dashed line, where L is the distance between the two mirrors. When a laser beam is incident parallel to the axis of the cavity it resonates within the cavity, as traced by the arrows, then is transmitted.

2.4 Interferometers for GW Detection

Michaelson interferometers are used in gravitational wave detection as a passing gravitational wave causes deformation of the arms, subsequently changing the length of the arms. A disturbance due to gravitational waves is expected to cause a change in arm length on the order of 10^{-18} m, a distance much smaller than the typical infrared wavelength of laser light used, meaning that the interferometer is highly sensitive to external vibrations as well as thermal noise of the mirrors creating slight changes in arm length, which is circumvented by placing the experiments in underground vacuums. The photons from the laser also introduce a shot noise which is reduced by using a high intensity beam [1].

Current experiments using interferometry include VIRGO and LIGO (Laser Interferometer Gravitational-wave Observatory), both of which consist of two underground Michelson interferometers created from suspended mirrors with arms between two and four kilometers long [1]. While these interferometers have yet to make a direct observation of a gravitational wave, collaborations have been able to place an upper limit on the SGWB in the frequency band around 100 Hz, ruling out some aspects of early universe models [7].

Another source of noise inherent in land based gravitational wave interferometers is gravitational noise from the Earth. Since the detector is built to be sensitive to tidal gravitational forces it cannot distinguish between those created on Earth, by matter interacting on or in the Earth, and weak signals originating in space. This limits the sensitivity range of such land detectors to high energy gravitational wave sources from space and for that reason, LISA (Laser Interferometer Space Antenna), was conceived [1]. Consisting of three space craft forming an equilateral triangle with arms $5 * 10^6$ km long, each satellite contains a test mass in free fall and emits two laser beams, connecting it to the other two satellites, resulting in a total of six laser links, as shown in Figure 6. The configuration is to orbit the sun about 20° behind the Earth and rotate once a year, as shown in Figure 7. LISA aims to detect gravitational waves in the $10^{-4} - 1$ Hz range, and achieve a sensitivity of detecting a gravitational deformation as small as $\approx 7 * 10^{-21}\sqrt{\text{Hz}}^{-1}$ around the frequency 5 mHz. With this frequency range and sensitivity LISA hopes to observe gravitational radiation from black holes, binary neutron stars as well as the Big Bang [13].

LISA's main challenges come from the ability of the spacecraft to follow the free falling test masses and of precise phase shift measurements. This later goal is made more difficult since the interferometer is not a classical Michaelson Interferometer which cancels out laser noise by recombining beams originating from the same laser, instead, LISA combines two beams originating from two different lasers, requiring highly frequency stabilized lasers and numerical algorithms to cancel the noise. Many laser stabilization methods have been considered, such as using a Fabry-Perot Cavity. This provides high stability over a short time period, however, the material of the cavity is subject to thermal and mechanical noise that is difficult to control, so a second solution was proposed, to stabilize the beam on a hyperfine transition of iodine which occurs at $\lambda = 532$ nm, exactly the second

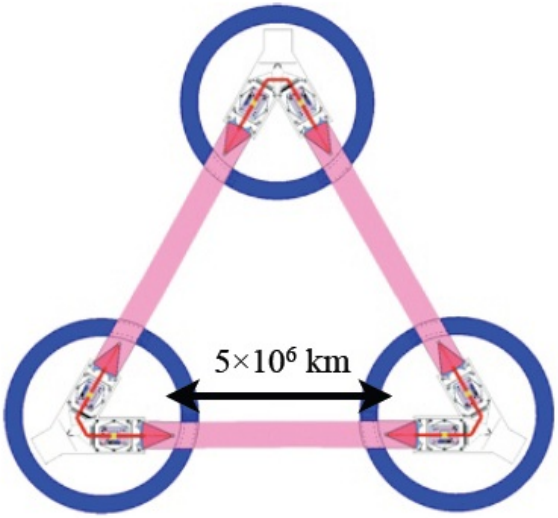

Figure 6: The basic configuration of LISA, three satellites are connected by six laser links in the formation of an equilateral triangle with arms around $5 * 10^6$ km long.

harmonic of the Nd:YAG lasers emitting at λ = 1064 nm used for the laser links of the satellites. This method is more effective than that of the Fabry-Perot Cavity as the iodine will be excited and emit at only one wavelength of light rather than introducing noise due to excess radiation built up from the beam resonating in the cavity. The goal of LASIC (Frequency Stabilized Laser to Iodine Lines for Space Applications) was to develop this method, and the goal of LASIC II, the apparatus for which is shown in Figure 8, is to improve upon the methods developed in the first project and bring the stabilization method closer to being space ready, namely, by making the stabilization apparatus compact enough to fit aboard a space craft.

3. Devices Characterized

Two important devices used in the LASIC II experiment, shown in Figure 8, are a fibered Evanescent Wave Coupler, which acts as a variable beam splitter and a fibered Electro-Optic

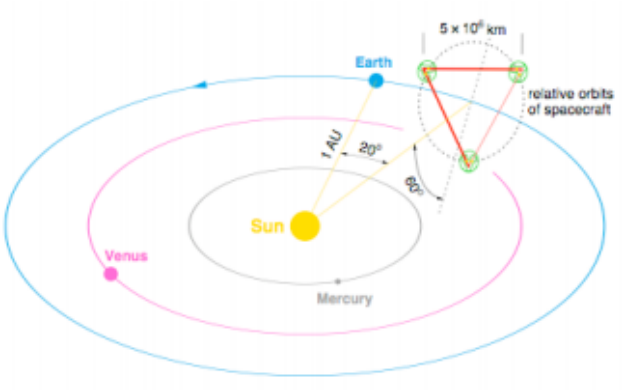

Figure 7: The location of the LISA satellites from Figure 6 in orbit around the Sun, approximately 20° behind the Earth.

Modulator, which introduces a phase shift to one of the split beams. Before the apparatus can be completed it was necessary to characterize these devices to be sure they would function properly in the experiment. While these two devices were the main goals of characterization, a non-fibered Acousto-Optic Modulator was also characterized for use in a heterodyne interferometry experiment to study the Electro-Optic Modulator.

3.1 Evanescent Wave Coupler (EWC)

An Evanescent Wave Coupler (EWC) is an optical waveguide that splits an input beam in varying ratios via the phenomenon of evanescent waves. In general, a waveguide is a device which guides the direction of propagation of waves, for example, a fiber optics cable uses the property of total internal reflection to guide electromagnetic radiation in the optical wavelength range. Total internal reflection occurs when light strikes a surface at an angle greater than the critical angle, as derived from Snell's Law, Equation 9, where n_1 and θ_1 are the index of refraction and angle of incidence of the light through the first material, and n_2 and θ_2 are the index of refraction and angle of transmission of the light through the second material [11], as shown in Figure 9.

$$n_1 \sin(\theta_1) = n_2 \sin(\theta_2) \quad (1)$$

If light passes from a material of higher index of refraction to a material with lower index of refraction, the light bends away from the normal, as shown in Figure 9, and if the refracted angle

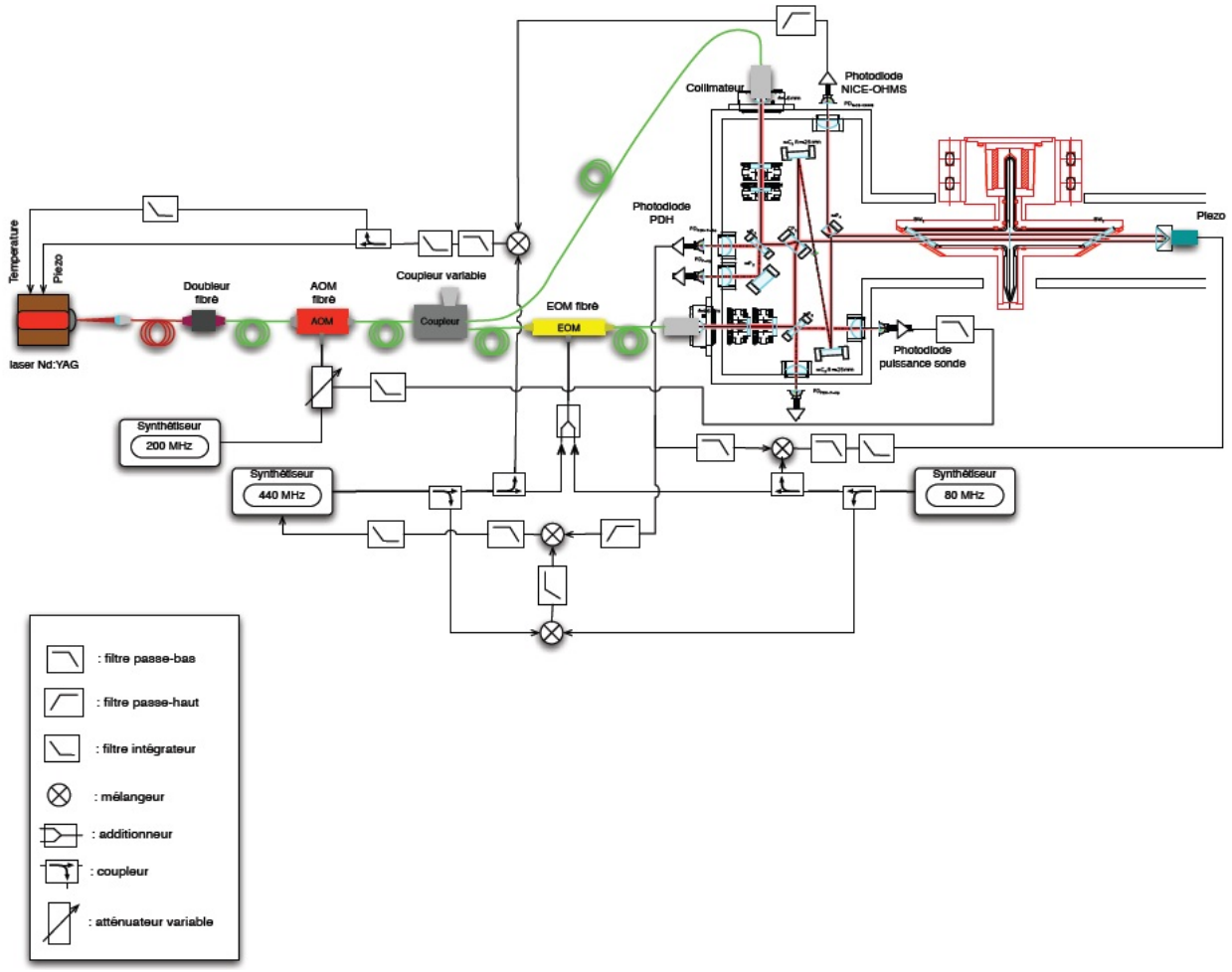

Figure 8: The proposed LASICII apparatus. A Nd-YAG laser emitting at λ = 1064 nm in the TEM_{00} mode is frequency doubled to λ = 532 nm by a fibered frequency doubling crystal. The beam is then split by an Evanescent Wave Coupler, where the evanescent beam is sent to the iodine cell to be stabilized by means of the hyperfine transition of iodine at its 532 nm line and the non-evanescent beam is phase shifted by a fibered Electro-Optic Modulator.The fiber optics devices allow for a compact apparatus, small enough to fit within a space craft.

is set to 90°, so that the light is reflected instead of refracted within the second material, Equation 1 can be solved for the critical angle, θ_c, also known as Bruster's angle, where the light is totally internally reflected within the second material [11], given by Equation 2.

$$\theta_c = \arcsin(\frac{n_2}{n_1}) \tag{2}$$

When light is totally internally reflected it cannot be discontinuous at the boundary of the medium of transmission, rather a portion of the light has an exponentially decaying probability to be transmitted instead of reflected, creating a second, less powerful beam whose amplitude decays exponentially as the distance from the medium of transmission is increased, called an evanescent wave. The electric field of the transmitted, evanescent wave, $\vec{E}_T$, is given by Equation 3 [14], where the real exponential shows an exponential decay in the $\hat{z}$ direction. An evanescent wave transmission is shown in Figure 10 [15].

$$\vec{E}_T = A_z e^{-\beta z} e^{i(\omega t - \frac{k_r \sin(\theta)}{n_r})} \tag{3}$$

An EWC utilizes evanescent waves to split an input laser beam by varying the distance be-

tween two monomode fiber optics cores, where the closer the cores the greater the evanescent wave transmission and as the cores are separated the evanescent wave transmission decreases.

The EWC studied in these experiments was made by Evanescent Optics Inc [16].

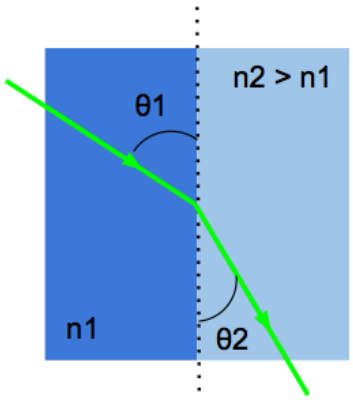

Figure 9: Light passing from a material with index of refraction, n_1, makes an angle of θ_1 with the normal, and is bent towards the normal at an angle of θ_2 when the index of refraction of the second material, n_2, is larger than the first.

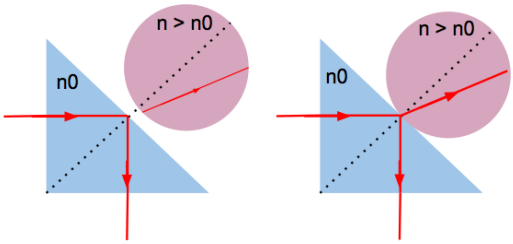

Figure 10: Example of an evanescent wave transmission. A beam is totally internally reflected within a fiber optics core, shown by the blue triangle, and a second fiber optics core, shown as a pink circle, receives a weak beam when the cores are further apart, as on the right, and a stronger beam when the cores are closest, as shown on the left.

3.2 Acusto-Optic Modulator (AOM)

The photo-elastic effect describes how applying a mechanical stress to a crystal changes it's permittivity, thus how it refracts optical light, or it's index of refraction. The acousto-optic effect makes use of this phenomenon by inducing mechanical stress on a crystal via a sound wave. A typical application of the acousto-optic effect is shown in Figure 11, where it is used to diffract an input beam by the Bragg angle, θ_B, as given in Equation 4, where λ is the wavelength of the input beam and Λ is the wavelength of the sound wave applied to the crystal.

$$\theta_B = \sin(\frac{\lambda}{2\Lambda}) \tag{4}$$

Figure 11 shows an Acousto-Optic Modulator (AOM), which is used to shift the input beam in frequency, also called a doppler shift, with the diffracted output beams, while the transmitted beam remains at the same frequency as the input beam. When an AC signal is applied to the Piezo-Electric Transducer, pressure waves are created which deform the crystal periodically, subsequently changing the index of refraction of the crystal in a periodic manner. The change in refractive index acts similar to a diffraction grating, resulting in a normally transmitted beam and diffracted beams at multiple harmonics, each separated by the angle given in Equation 4 [17].

The AOM studied in these experiments was made by AA Opto-Electric [18].

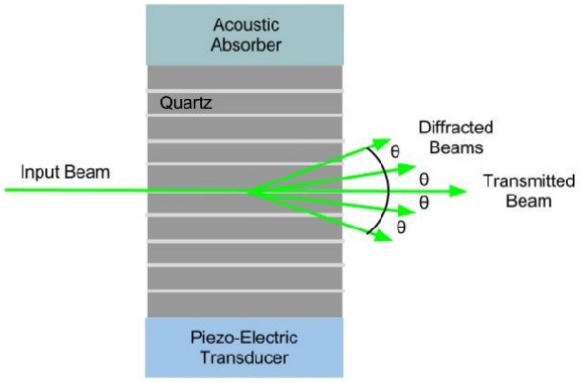

Figure 11: Basic schematic of an Acusto-Optic Modulator. An AC signal is applied to the Piezo-Electric Transducer, deforming the crystal and creating pressure waves which in turn deform the quartz crystal, periodically changing it's index of refraction, causing an input optical laser beam to be diffracted.

3.3 Electro-Optic Modulator

The purpose of the Electro-Optic Modulator (EOM) in the LASIC II experiment is to introduce a phase shift to the input beam, which is achieved by means of the linear electro-optic effect. Similar to the acousto-optic effect which introduces a change in refractive index to a crystal by means of an acoustic wave, the electro-optic effect introduces a change in refractive index to a crystal by means of an applied electric field. Quantitatively the electro-optic effect is given by Equation 5, where n is the index of refraction in the material altered by the electro-optic effect, n_0 is the index of refraction of the material before an electric field is applied to the material, a is the linear electro-optic effect, and E_0 is the applied electric field.

$$n = n_0 + aE_0 + bE_0^2 + ... \tag{5}$$

The second order term in Equation 5, bE_0^2 is called the Kerr Effect, whereas the first order term, aE_0 is the linear electro-optic effect, the underlying principle of how the EOM functions.

The electric field applied to the crystal is defined in terms of the voltage applied perpendicular to the polarization vector of the input beam, V_s, by Equation 6,

$$E_0 = \frac{V_s}{d}, \tag{6}$$

which allows for the phase shift induced on an input beam, $\Delta\phi$, to be solved for in terms of the voltage applied to the device by Equation 7,

$$\Delta\phi = 2\pi k a V_s. \tag{7}$$

An important characteristic of the EOM is the half-wave voltage or V_π, the applied voltage needed to introduce a phase shift of π to the input beam [17]. It is also important to note that the input beam to the EOM must be of the correct polarization, otherwise the device will not function properly. Since the voltage to create the electro-optic effect must be applied perpendicular to the polarization vector, the input beam must not only be linearly polarized but at the correct angle. Without the correct angle of polarization insertion losses of around 20 dBm were obtained, however, once the polarization angle was changed by a $\frac{\lambda}{2}$ waveplate, the polarization vector of the input beam was perpendicular to the applied voltage and insertion losses of 5 dBm were obtained, better than the manufacturer's claims of 7 dBm.

The EOM used in these experiments was made by Jenoptik [19].

4. Polarization

Each of the three devices studied, the Evanescent Wave Coupler, the Acousto-Optic Modulator and the Electro-Optic Modulator, are polarizing maintaining, according to their manufacturers, and since interferometry requires consistently polarized beams it was necessary to verify that each device maintains the linear polarization of the input beam. While the device must be polarizing maintaining, it does not have to maintain the angle of polarization as that is easily controlled with a half-wave plate.

4.1 Background

Light, as a transverse electromagnetic wave, contains an electric and a magnetic field which propagate perpendicular to one another. The polarization of light is a property of the electric field vector's orientation, such that by projecting the electric field vector, $\vec{E}$, onto the cartesian coordinates, $\hat{x}$ and $\hat{y}$, the relative magnitude and angle between the $\hat{x}$ and $\hat{y}$ components determines the polarization of light. For example, if the electric field of an electromagnetic wave creating a laser beam is described by Equation 8,

$$\vec{E} = \hat{x}E_{o_x}\cos(kz-\omega t) + \hat{y}E_{o_y}\cos(kz-\omega t+\theta), \tag{8}$$

where E_{o_x} and E_{o_y} determine the amplitude of the EM wave and θ is the phase shift between the $\hat{x}$ and $\hat{y}$ components, then the polarization of the laser is determined by θ and the relative magnitudes of E_{o_x} and E_{o_y}.

Light is considered linearly polarized if $\theta = 0, \pi$ as there is no phase shift between the $\hat{x}$ and $\hat{y}$ components of the electric field, thus the two components are oscillating about a line, as shown in Figure 12a. If, however, there is a phase shift

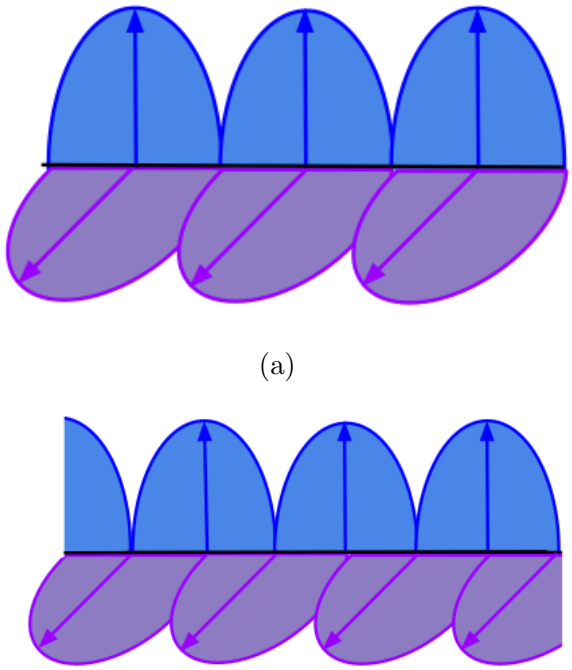

(a)

(b)

Figure 12: The electric field components, E_x and E_y, are of equal magnitude for both linearly and circularly polarized light, however, there is a phase shift of $\theta = 0$ for linearly polarized light (a), and a phase shift of $\theta = \pm\frac{\pi}{2}$ for circularly polarized light (b).

of $\theta = \pm\frac{\pi}{2}$ between the two components of the electric field and each component has the same magnitude, $E_{o_x} = E_{o_y}$, then the light is considered to be circularly polarized as the phase shift causes the electric field vector to trace out a circle in the x-y plane, as shown in Figure 12b [20].

If the $\hat{x}$ and $\hat{y}$ components of the electric field have any phase shift other than $\theta = 0, \pm\frac{\pi}{2}$, and if $\theta = \pm\frac{\pi}{2}$ but the amplitudes of the components are not equal, such that $E_{o_x} \neq E_{o_y}$, the light is considered to be elliptically polarized as the electric field vector can trace an ellipse in the x-y plane with any major to minor axis ratio at any arbitrary angle, a shown in Figure 13 [20].

4.2 Polarizers and Waveplates

Two useful tools in studying the polarization of light are polarizers and wave-plates, also called phase retarders.

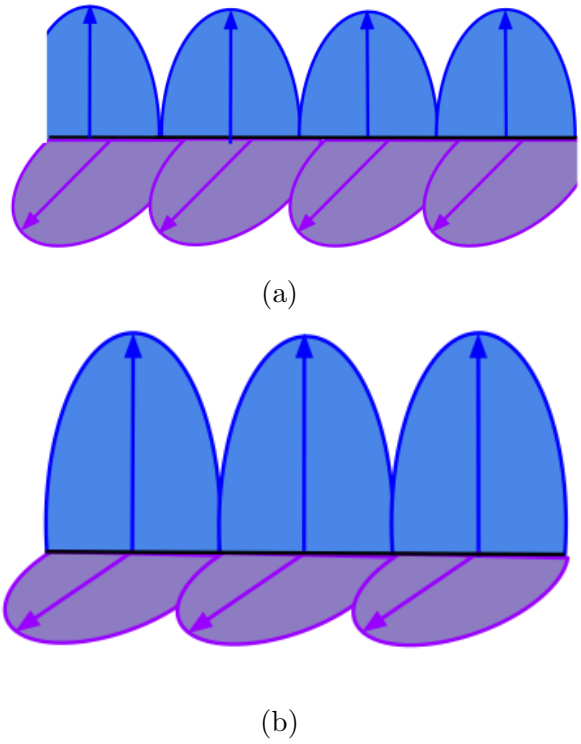

(a)

(b)

Figure 13: The electric field components, E_x and E_y for elliptically polarized light can be of any phase shift other than $\theta = 0, \pi, \pm\frac{\pi}{2}$ (a) and any relative amplitude (b).

One means of producing polarized light is by reflection and transmission, since light reflected from a smooth surface at a non-zero angle of incidence becomes partially polarized. The light which is transmitted through the plane is called π light, as it's electric field is parallel to that of the plane, and the reflected light is called σ light, as it's electric field is perpendicular to the plane and cannot be transmitted. By stacking many such plates a plate polarizer is created, where changing the angle of incidence upon the plate polarizer changes how much light is transmitted and how much is reflected. Thus, changing the angle can result in all π light, where there is complete transmission through the polarizer, called a maximum of transmission, or in all σ light, where there is complete reflection off of the plate polarizer, called a minimum of transmission, or in partial transmission and partial reflection [20]. By studying the amount of light transmitted through a polarizer the polarization of the light can determined.

While polarizers allow the polarization of an incident beam to be studied, wave-plates actively alter the polarization of an incident beam. Wave-plates are also known as phase retarders as they change the relative phase between components of the electric field. A typical method for creating a wave-plate is using quartz crystal, where the optical axis is positioned such that the incident polarized light is resolved into it's components, thus creating a phase shift between them when they exit the crystal. The phase shift is proportional to the thickness of the plate, thus it is also dependent upon the wavelength of the incident light, such that a wave-plate that acts as a $\frac{\lambda}{4}$ for λ = 1064 nm light will act as a $\frac{\lambda}{2}$ for λ = 532 nm light.The difference between these two types of wave-plates is that a $\frac{\lambda}{4}$ will not only change the angle of polarization but turn elliptically or circularly polarized light to linearly polarized light, whereas a $\frac{\lambda}{2}$ wave-plate will only change the angle of polarization. Thus, by using the two plates in conjunction with one another it is possible to finely control the linear polarization of light and the angle at which that polarization occurs when observed through a plane polarizer [17].

4.3 Experimental Methods

To verify that each device studied was indeed polarizing maintaining, that is each device's output beam preserved the linear polarization of the input beam, the basic apparatus shown in Figure 14 was used. For the fibered devices, the EWC and the EOM, it was necessary to bring the beam from the fiber optics cable to open air in order to use the plane polarizer, thus a mounted fiber optics coupler was used. A plane mirror directed the beam through a plane polarizer whose output was read on a photodiode. The information from the photodiode was then sent to an oscilloscope and read through a LabVIEW program run from the computer to which the oscilloscope was connected. To measure the polarization of the non-fibered devices, such as the AOM, the coupler was not used and the output from the device was directly sent through the polarizer.

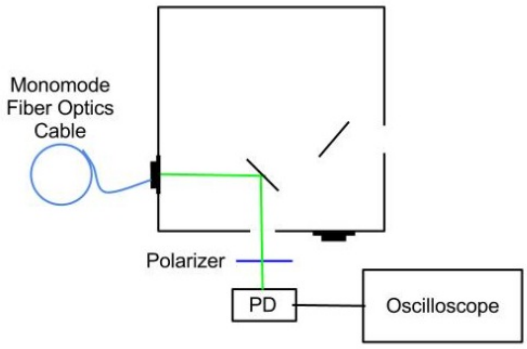

Figure 14: Basic apparatus used to measure the polarization of fibered devices. The beam is brought from the monomode fiber optics cable to open air by use of a coupler, the free beam is then directed to a plane mirror, through a plane polarizer, whose output is sent to a photodiode, marked PD. The output from the photodiode is then read by an oscilloscope.

To find the polarization of a beam incident upon the plane polarizer, the angle marked on the polarizer was changed in increments of 10° or 20° and the photodiode recorded the subsequent change in power at each angle. As power is proportional to voltage, the voltage read by the oscilloscope and recorded in LabVIEW reflects the change in power as the polarizer angle is altered.

4.4 LabVIEW Program

The LabVIEW program used to collect data utilized the drivers provided by the manufacturer to communicate with the Tektronix AFG 3252 oscilloscope. A spreadsheet was initialized outside of a stacked sequence, where first a data point is collected from three different channels or types of measurements, then each of the three data points are added to the spreadsheet by changing the data point type from double precision to a string, loosing a small amount of precision but not significantly such that it added error to the measurements. The block diagram of the program is shown in Figure 15. The main asset of using LabVIEW was to provide multiple accurate measurements of the power transmitted by the polarizer, allowing the average power to

be measured for each polarizer angle, where the standard deviation of the power measurements gave an estimate of error.

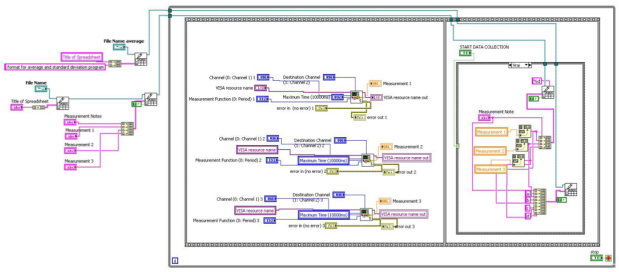

Figure 15: Image of the block diagram of the LabVIEW program used to record three channels of data from a Tektronix AFG 3252 oscilloscope into a spreadsheet.

4.5 Data Analysis

Once the raw data was collected, the mean power value and standard deviation from the mean were calculated for each angle of the polarizer, giving a value and it's error for each point.

To determine if the beam studied was linearly polarized Malus' Law, Equation 9 [11], was used.

$$P = P_o \cos^2(\theta) \tag{9}$$

Malus' Law states that the power of a linearly polarized beam transmitted through a polarizer, P, is equal to the power incident upon the polarizer, P_o, multiplied by the Cosine squared of the polarizer angle, θ. However, the equation only applies when the angle at which the maximum power is transmitted is defined as $\theta = 0$. This was achieved by taking the raw data, as shown in blue in Figure 16, finding the first maximum angle, then shifting each angle by that amount, obtaining the same trigonometric relationship as before, however shifted by a slight angle, as shown by the red curve in Figure 16.

A linear relationship between P and $\cos^2(\theta)$ demonstrates that the beam is linearly polarized, while the extinction ratio of the beam demonstrates the quality of the polarization. The extinction ratio of an optical beam can be defined in many ways, where one common means is to use a decibel system and report the ratio in units of dBm. This method is defined in Equation 10,

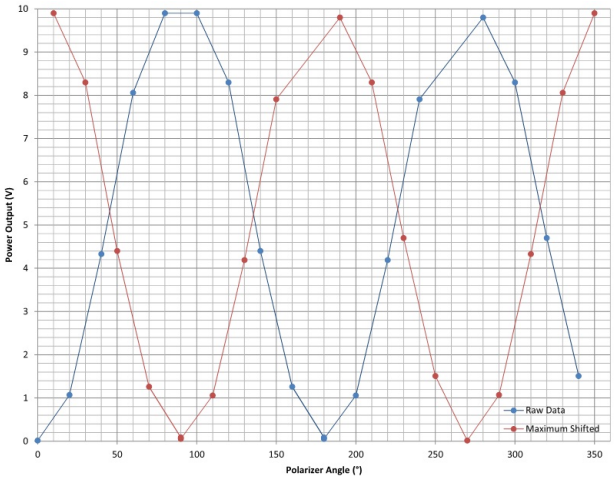

Figure 16: Polarization data taken on unaltered LASIC II beam. The blue curve displays the data at the arbitrary angles measured on the plane polarizer. The red curve displays the data at the angles shifted such that the maximum occurs at $\theta = 0$.

where P_{min} is the minimum power transmitted through the polarizer and P_{max} is the maximum power transmitted through the polarizer. The larger the ratio the higher the quality of the linear polarization as it means that the beam is well extinguished at the minimum power transmission and well transmitted at the maximum.

$$Log_{10}(\frac{P_{min}}{P_{max}}) \tag{10}$$

4.6 Results

In order to determine if the various beams followed Malus' Law and thus were linearly polarized, the power detected at the photodiode, normalized by dividing by the maximum power transmitted, was plotted against the $\cos^2$ of the shifted polarization angle, θ. A linear relationship conveys that the beam is linearly polarized as it follows Malus' Law, Equation 9, and is displayed in Figure 17 where the output beams from the Evanescent Wave Coupler, the Acousto-Optic Modulator and the Electro-Optic Modulator, are each linearly polarized as each displays a linear relationship following Malus' Law.

The extinction ratio's of the three devices were then calculated to be 17.5 dBm for the AOM, 30 dBm for the EOM, 30 dBm for the non-evanescent beam of the EWC and a range

of 25 - 33 dBm for the evanescent beam as the coupling ratio is raised from the minimum to the maximum.

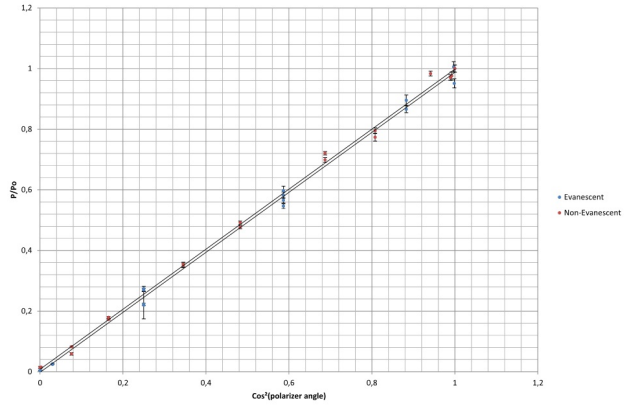

a

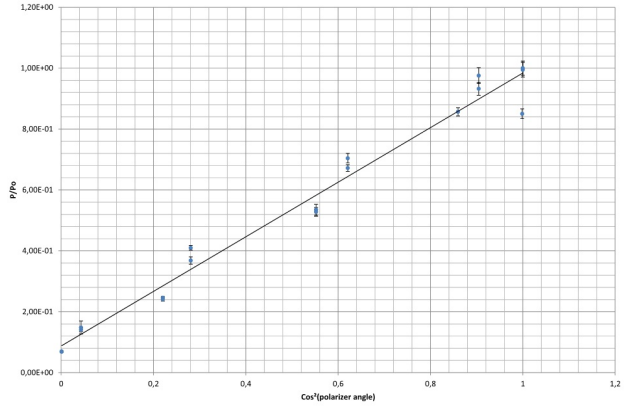

b

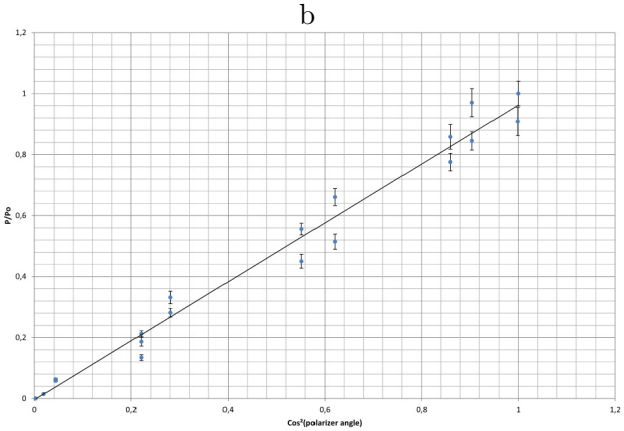

c

Figure 17: The linear relationship following Malus' law indicates that the output beams from a.) the Evanescent Wave Coupler, b.) the Acusto-Optic Modulator and c.) the Electro-Optic Modulator are linearly polarized.

5. Coupling Ratio of Evanescent Wave Coupler

The purpose of the EWC in the LASIC II experiment, as shown in Figure 8, is to split the frequency doubled beam originating from the Nd:YAG laser. Due to the EOM's high insertion loss, around 5 dBm, it is necessary to split the beam into unequal parts, with the highest intensity beam input to the EOM so that when the two beams are recombined they are of nearly equal power. The best ratio of beam intensities needed for the apparatus is not known so it is desirable to use a variable splitter to add flexibility to the apparatus design. One way to characterize how the coupler splits the beam is by the coupling ratio, given by Equation 11, as the ratio of the intensity of the evanescent beam in comparison to the non-evanescent beam.

$$\text{coupling ratio} = \frac{I_{\text{Evanescent}}}{I_{\text{Non-Evanescent}}} \tag{11}$$

5.1 Experimental Methods

The experimental apparatus used to measure the coupling ratio of the EWC is given in Figure 18, where the beam to be split is input into the EWC, then each beam is brought from the fiber optics cable to open air by a coupler. Two plane mirrors then direct each open air beam to a separate photodiode which is read on an oscilloscope. The LabVIEW program used in the polarization experiment was again used to collect information on the relative powers of the split beams.

A micrometer knob on the body of the EWC alters the position between the two fiber optics cores within the device, consequently changing the coupling ratio, as the power of the Evanescent beam is at maximum when the two cores are closest together and diminishes when the cores are brought further apart. By changing the position of the micrometer knob and recording the subsequent change in the two beam's powers using the LabVIEW program, the coupling ratio was found, as shown in Figure 19.

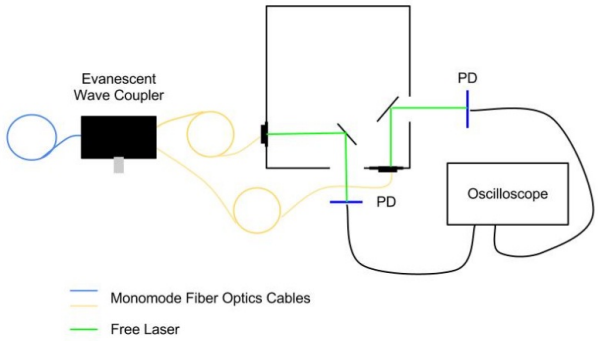

Figure 18: The basic apparatus to measure the coupling ratio of the fibered Evanescent Wave Coupler. The beam input to the blue, monomode fiber optics cable is split into an Evanescent and Non-Evanescent beam, represented by the yellow fiber optics cables. The beams are brought to open air by two couplers, then are guided to photodiodes (PD) by plane mirrors. The output from the photodiodes is then read on an oscilloscope. The grey knob on the EWC's black body represents the micrometer which varies the coupling ratio.

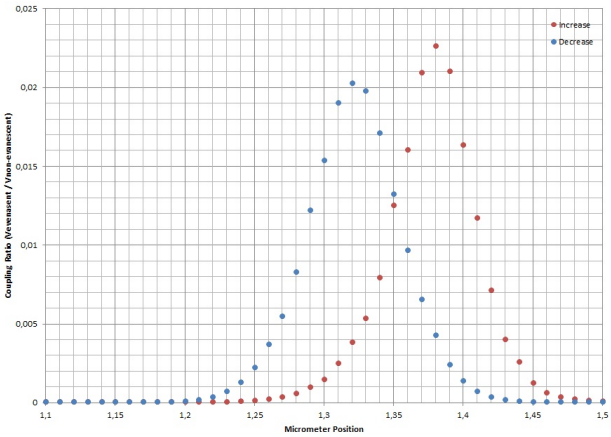

Figure 19: Graph displaying the mechanical hysteresis of the EWC. The horizontal axis is the micrometer position, as defined by the numbers displayed on the knob, and the vertical axis displays the coupling ratio. Under different conditions of finding the maximum evanescent wave output the micrometer position where the maximum occurs changes, where if the position is increased the maximum occurs at the micrometer position 1.38 and if the position is decreased, the maximum occurs at 1.32.

5.2 Mechanical Hysteresis

The LabVIEW program collects multiple data points at each micrometer position and taking an average of all the original points collected then computing the coupling ration, Equation 11, reveals the relationship between the coupling ratio and micrometer position shown in Figure 19. The blue curve corresponds to the condition when the micrometer position is set to a point beyond the maximum evanescent wave output, beginning at the position defined as 1.5, then decreasing the position to 1.1. The red curve corresponds to the inverse condition, where the micrometer position is begun at a low position, such as 1.1, and is increased past the maximum to the position 1.5. Under these two conditions the micrometer position where the evanescent wave output is maximum changes, where for the decreasing condition the maximum output occurs at the position 1.32 and for the increasing condition the maximum output occurs at the position 1.38.

The two maximum positions indicate the presence of a mechanical hysteresis in the micrometer knob, meaning that the position of the knob cannot be relied upon to find the maximum ouput, unless if the exact conditions presented in Figure 19 are repeated. Similarly, searching for the maximum by increasing and decreasing the micrometer position between, for example, positions 1.3 and 1.4, results in a typical hysteresis curve, where the maximum position alternates between the positions 1.32 and 1.38.

It is not unexpected for the EWC to display such a hysteresis, as the manufacturer states that the micrometer position should not be relied upon to find the maximum evanescent wave output. However, it is important to note when searching for the evanescent wave's maximum output, as the location of the maximum changes once it has been passed, making it necessary to approach the maximum location and stop near the maximum output. The only potential problem is that it appears the hysteresis does not result in a steady maximum, since the maximum coupling ratio for the maximum at 1.38 is larger than for the maximum at 1.32. It is not ideal

that the coupling ratio changes by the method of finding the maximum evanescent wave output, however, now that it is known, it is simple to find the maximum output ratio following the method of increasing the micrometer position from a distance far away from the maximum and stopping one the coupling ratio has reached around 0.0225.

6. V_π of Electro-Optic Modulator

In the LASIC II experiment, the EOM introduces a phase shift to the non-Evanescent beam split from the original, frequency doubled beam, as shown in Figure 8. In order to understand how the EOM performs this phase shift, an important characteristic of the device is V_π, the voltage needed to introduce a phase shift of π to the input beam. The manufacturer claims that at around 1 kHz V_π = 3.2 V, and the following experiment set to test this and find how V_π changes with the frequency of modulation of the EOM. The goal of the experiment is to split the original beam with the EWC, then introduce a phase shift with the EOM to one beam and frequency shift the second beam with the AOM, then recombine the two beams and use the beat frequencies produced by the heterodyne interferometry to fit a model of the expected results, which depends upon V_π.

6.1 Theoretical Model

The heterodyne interferometry apparatus is similar to the Mach-Zhender Interferometer described in Section 2.3, as it involves interfering two beams derived from the same laser, however, one beam has been frequency shifted, which produces a beat frequency in the interfered beams.

Beats occur when two waves, such as sound light waves, with slightly different frequencies are interfered, creating periodic variations in the volume, for sound waves, or intensity, for light, that are called beats. Figure 20 shows the interference of two such waves in black, where the frequency of the successive minima and maxima is the frequency difference of the source waves.

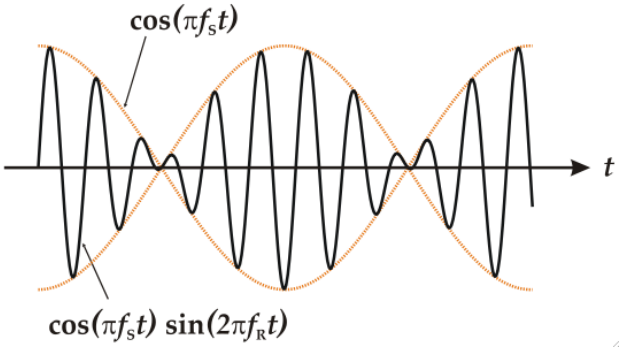

Figure 20: Example of beats, achieved by interfering two waves with slightly different frequencies.

In the heterodyne interferometer used in this experiment the electric field of the beam phase shifted by the EOM can be described by Equation 12, where $\vec{E}_o$ is the amplitude of the electric field, ω_0 is the optical frequency of the beam, β is a constant called the modulation index, and Ω is the RF frequency at which the EOM is driven, thus the frequency which was varied throughout the experiment.

$$\vec{E}_{\text{EOM}} = \vec{E}_o e^{i(\omega_0 t + \beta \sin(\Omega t))} \tag{12}$$

The electric field, Equation 12, can then be rewritten as Equation 13,

$$\vec{E}_{\text{EOM}} = \vec{E}_o e^{i\omega_0 t} e^{i\beta \sin(\Omega t))}, \tag{13}$$

where the second complex exponential portion of the electric field can be written as a sum of Bessel Functions, as given in Equation 14.

$$e^{i\beta \sin(\Omega t))} = \sum_{n=-\infty}^{n=+\infty} J_n(\beta) e^{in\Omega t} \tag{14}$$

The electric field of the beam doppler shifted by the AOM can then be described by Equation 15, where ω is the frequency at which the AOM is modulated.

$$\vec{E}_{\text{AOM}} = \vec{E}_o e^{i(\omega + \omega_o)t} \tag{15}$$

It is then known that the intensity of the signal received at the photodiode, thus the intensity of the interfered phase and frequency shifted beams, is proportional to the sum of the two electric fields by Equation 16.

$$I_{\text{PD}} \propto | \vec{E}_{\text{EOM}} + \vec{E}_{\text{AOM}} |^2 \tag{16}$$

Then by substituting the electric field of the EOM, Equation 13, with the Bessel Function approximation, Equation 14, and the electric field of the AOM, Equation 15, it can be calculated that the intensity of light detected at the photodiode is proportional to the Bessel Function approximation to first order as given in Equation 17.

$$I_{\mathrm{PD}} \propto J_0(\beta)\cos(\omega t) + J_1(\beta)[\cos((\omega-\Omega)t) - \cos((\omega+\Omega)t)]... \quad (17)$$

The first three Bessel Functions in Equation 17 show that the first three beat frequencies occur at ω for the zeroth order, J_0, and $\omega \pm \Omega$ for the first order, J_1.

In order to relate Equation 17 to experimental data, recall that the intensity of the light incident upon the photodiode is related to the power of the beam by Equation 18, where A is the area the light covers.

$$I = \frac{P}{A} \quad (18)$$

Then power is related to the voltage read by the oscilloscope by Equation 19, where R is impedance of the load to the oscilloscope, in this case $R = 50\Omega$, as specified by the photodiode used in the apparatus.

$$P = \frac{V^2}{2R} \quad (19)$$

Finally, the characteristic V_π is related to the interfered electric fields through the modulation index, β, by Equation 20, where V_{RF} is the amplitude of the RF signal modulating the EOM.

$$\beta = \pi \frac{V_{RF}}{V_\pi} \quad (20)$$

6.2 Experimental Methods

The experiment was performed using the apparatus shown in Figure 21. A Nd:YAG laser produces a beam in the TEM_{00} mode at $\lambda = 1064$ nm, which is frequency doubled using a non-fibered frequency doubling crystal. The free beam is then guided to through a $\frac{\lambda}{2}$ waveplate set at an angle of $\theta = 86°$ to control the angle of polarization and allow the EOM to function properly. A lens with a focal length of 100 mm, followed by an aperture and a second lens with a focal length of 50 mm focuses the beam at a coupler which brings the beam into a monomode fiber optics cable. The Evanescent Wave Coupler splits the beam from the monomode fiber optics cable into a non-evanescent and evanescent beam. The non-evanescent beam is brought to a fibered Electro-Optic Modulator, which introduces a phase shift to the beam at the same frequency of the signal from the signal generator driving the EOM. The amplitude of the signal applied to the EOM determines the amplitude of the modulation the EOM provides to the input beam. The evanescent beam is then brought to a coupler which brings the beam from the fiber optics cable to open air. Two waveplates, a $\frac{\lambda}{4}$ set at an angle of $\theta = 249°$ and a $\frac{\lambda}{2}$ set at an angle of $\theta = 302°$ control the polarization of the beam. A plane mirror then guides the free beam to a non-fibered Acusto-Optic Modulator, which introduces a frequency shift to the beam equal to the frequency at which the function generator is driving the AOM. In this experiment, the AOM was always driven at 80 MHz. The amplifier serves to amplify the driving signal before it reaches the AOM in order to increase the intensity of the first diffracted beam output by the AOM. An aperture then selects the first diffracted beam from the output of the AOM, blocking the transmitted beam as well as all other harmonics. Similarly, the output from the EOM is sent to a coupler, which brings the beam from the fiber optics cable to open air, where it's polarization is controlled by means of two waveplates, a $\frac{\lambda}{4}$ set at an angle of $\theta = 94°$ and a $\frac{\lambda}{2}$ set at an angle of $\theta = 14°$. The beam is then directed to a beam splitting cube by means of two mirrors, to be interfered with the first diffracted beam output from the AOM, whose position is also controlled by two mirrors. The interfered beam exiting from the BS cube is focused on a fast-photodiode by a lens with a 15 mm focal length. The signal from the FPD is then amplified and read on a spectrum analyzer, which captures the beats created by the interference of the phase and frequency shifted beams.

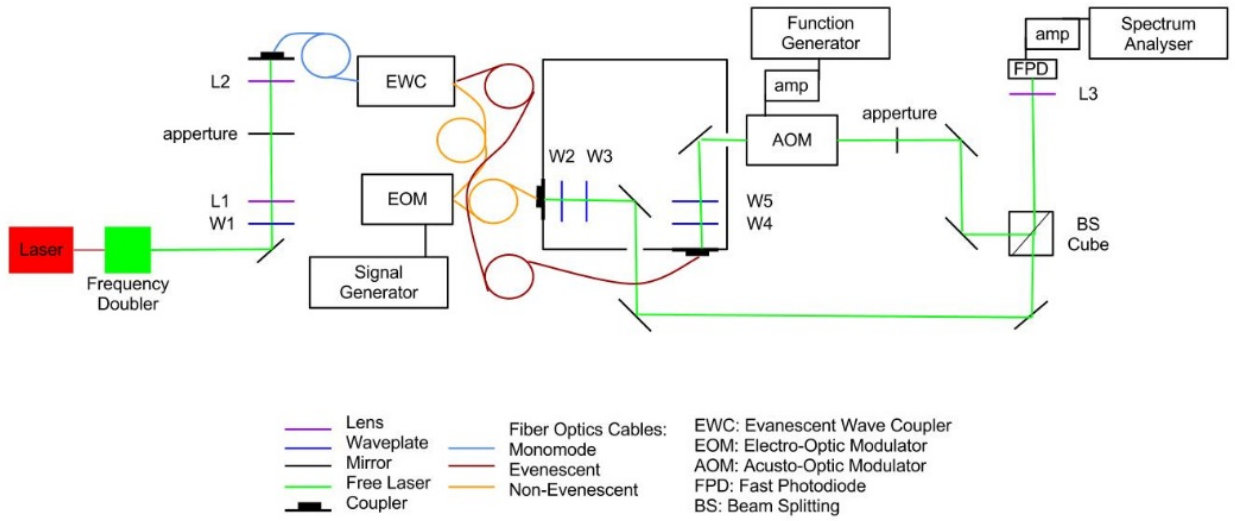

Figure 21: The apparatus used to perform heterodyne interferometry. The beam is created by a Nd:YAG laser at $\lambda = 1064$ nm, which is doubled in frequency by a non-fibered frequency doubling crystal. The beam is then sent through a $\lambda/2$ waveplate to control the angle of polarization. Focusing lenses and an aperture bring the beam from a coupler to a monomode fiber optics cable. The EWC then splits the beam, where the non-evanescent beam is sent to the EOM and the evanescent beam is brought to the AOM. Waveplates W2 through W5 ensure that the beams exiting from the AOM and EOM are both linearly polarized at the same angle once they exit from the beam splitting cube. The two beams are directed to the BS cube by four plane mirrors where they are interfered and one half of the recombined beam is sent through a small focusing lens to a Fast-Photodiode, whose signal is amplified and read by a Spectrum Analyzer.

In order to observe beat frequencies on the spectrum analyzer the beams from the AOM and EOM must be perfectly aligned, which was achieved using a variety of methods. Aligning the beams by eye sight gives a rough approximation of their locations. Then reading the photodiode into an oscilloscope allows for the signals amplitudes to be maximized, so that each beam is well aligned on the photodiode. Finally, a beam camera, connected to a computer and run from the program, DataRay, provides a precise location of the beam on it's CCD captors, and placing both beams in the same location on the CCD means that they are interfering well, as seen in Table 1. Once the beats are observed on the spectrum analyzer, final adjustments can be made to maximize the signal observed, though these are usually slight. An example of beat frequencies observed is given in Table 2.

Once the apparatus was complete, data was taken by selecting a frequency of EOM modulation and varying the RF level of the modulation signal. The EOM can receive a signal of 5 V amplitude at maximum, thus each data set begun at the maximum allowed voltage and decreased the RF level of modulation until the first harmonic beats were reduced to the noise threshold of the photodiode. Since the model to fit the data and find V_π requires only the first order approximation of the Bessel functions, only the peak amplitudes of the principle peak, at ω = 80MHz, and the first harmonic peaks at $\omega \pm \Omega$ were recorded. The peak amplitudes were measured using the peak search function of the spectrum analyzer and five readings were taken for each peak at each RF level of modulation. Taking the average of these data points provided the mean, which was used in data analysis, and the standard deviation from the mean of the raw data provided the error of each measurement.

6.3 Data Analysis

Once the mean and standard deviation of the raw data is calculated, it is important to check the quality of the data set which can be quickly assessed by observing how stable the peaks are.

(a) 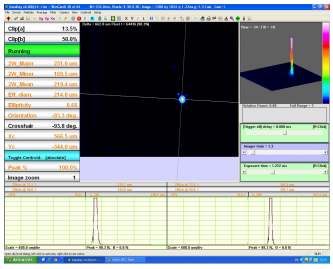 (b) 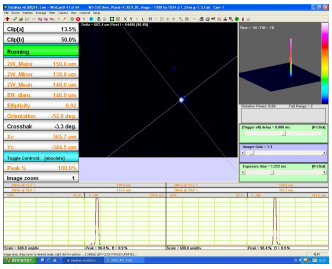 (c) 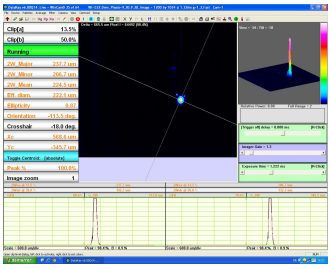

Table 1: Screenshots of the DataRay program observing the position of the beam from the (a) EOM, the (b) AOM and (c) the interfered beam.

(a) 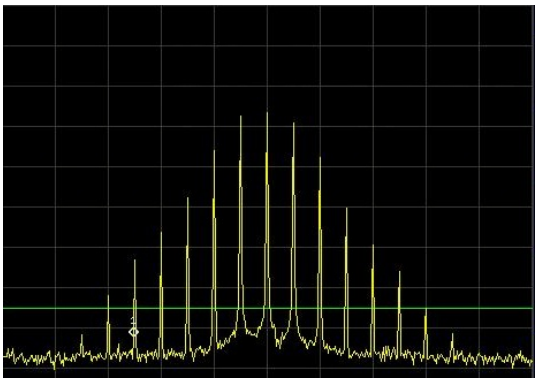 (b) 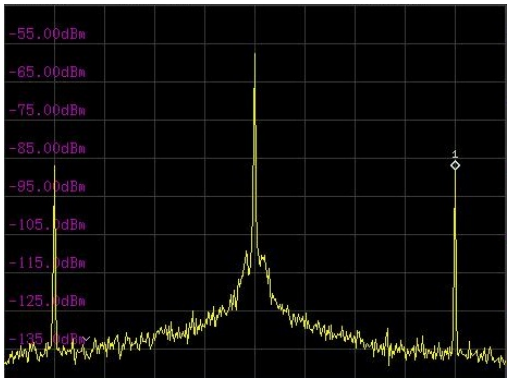

Table 2: Example of beat frequencies obtained from the heterodyne interferometry experimental apparatus in Figure 21 where $\omega = 80$ MHz and $\Omega = 40$ kHz. a.) The EOM is driven at an RF amplitude of +10 dBm and the beat frequencies descend from the principal peak every 40 kHz. b.) The EOM is driven at an RF amplitude of -15 dBm where the first harmonic peaks are pictures at 79.96 MHz and 80.04 MHz.

Ideally, the principle peak is consistent in amplitude as the RF level of modulation is changed since the two quantities are not supposed to be interdependent. It is also important that the two first harmonic peaks have nearly the same amplitude throughout a data set, as they theoretically should be of the same amplitude. When these conditions are met the data set is good and the average of the two first harmonic peaks was taken in order to be analyzed. An example of good peak stabilities is shown in Figure 22.

Each peak was measured on the spectrum analyzer in decibel units, dBm, which is related to the power detected on the photodiode in mW, P, by Equation 21.

$$\text{dBm} = 10\log_{10}(P) \tag{21}$$

The power of the beam is then converted to volts by Equation 22, rearranged from Equation 19, where only the positive root is used as negative voltage does not make physical sense for this apparatus.

$$V = \sqrt{2RP} \tag{22}$$

In addition to measuring the peak amplitudes on the spectrum analyzer, for each data set the noise level due to the photodiode was measured, in addition to any extra noise at the central peak location when only the beam from the AOM was incident upon the photodiode instead of the interfered beam. These values were also converted to mV using Equations 21 and 22. The noise level was then subtracted from each of the three peaks measured and the principle peak noise was subtracted from the principle peak only. Next, the ratio of the first harmonic peak amplitude to the amplitude of the principle peak was calculated. Plotting this on a log-log scale against the RF level of modulation of the EOM results in a linear relationship, as shown in Figure 23. The linear relationship was useful to compare the experimental data to the theoretical model, also

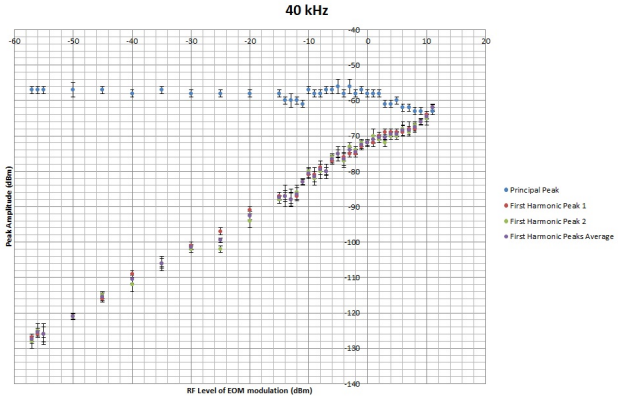

Figure 22: The peak amplitudes of the principle and first harmonic peaks and how they change with RF level of modulation when the EOM was driven at a frequency of 40 kHz. The blue curve represents the principle peak, the red curve represents the first harmonic peak at 79.96 MHz, the green curve represents the first harmonic peak at 80.04 MHz, and the purple curve represents the average of amplitude of the first harmonic peaks.

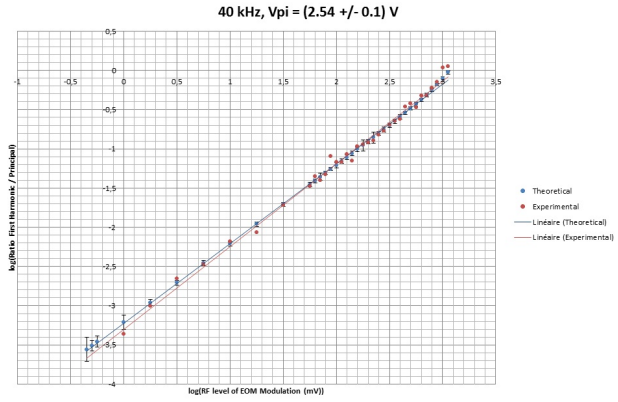

Figure 23: The raw experimental data has been converted from dBm to mV, from which the noise threshold of the photodiode was subtracted and the ratio of the first harmonic peak to the principle peak was calculated. The experimental data is compared to the theoretical model on a log-log scale, revealing a linear relationship. The value of V_π that best fits the experimental data when the EOM is driven at a frequency of 40 kHz is $V_\pi = 2.54 \pm 0.1$ V.

shown in Figure 23. The Bessel Functions were calculated using the built-in functions of Excel, where a value of V_π was selected by controlling the modulation constant, β, and how well the theoretical model matched the experimental data was determined by eye-sight, observing when the two linear relationships were most similar. The error was determined by how much V_π could change while still convincingly matching the experimental data.

The experimental data fit to the theoretical model for all data points taken is presented in Appendix A.

6.4 Results

By varying the frequency at which the EOM was modulated and calculating the subsequent change in V_π, the relationship between the EOM frequency of modulation and V_π shown in Figure 24 was found. The blue data points were analyzed in the method outlined in the previous section whereas the red and green data points were analyzed using a χ^2 fitting program in GnuPlot and the V_π of each first harmonic peak was found separately, instead of finding the V_π which matches the average of the two peaks. While these two methods results in slightly different values of V_π and the values are not always the same within error, it is important to note that they appear to follow the same trend, a potentially exponential curve as the frequency of EOM modulation increases, meaning that the results from the two methods are consistent.

The dependance of V_π upon the frequency of EOM modulation is unexpected as the manufacturers makes no mention of the possible relationship. Additionally, the manufacturer states that at a modulation frequency of 1 kHz V_π should be 3.2 V, which is inconsistent with the experimental data as V_{pi} at low frequencies plateaus around 2.5 V, however, this inconsistency is not a large concern as the voltages are relatively similar and within the range of the EOM's maximum applied voltage. What is concerning is the large values of V_π found at higher frequencies, specifically around 300 MHz when V_π jumps above 5 V and rises exponentially to 13.5 V at 750 MHz. If V_π actually rises this high for these frequencies it indicates that a full phase modulation cannot be achieved as it would require applying a voltage of an amplitude beyond what is safe for the device. This is not ideal as the LASIC II experiment would like to modulate the EOM between

the frequencies 40 kHz and 440 MHz, and currently it appears that the EOM will not achieve a full phase modulation at the higher end of the frequency range.

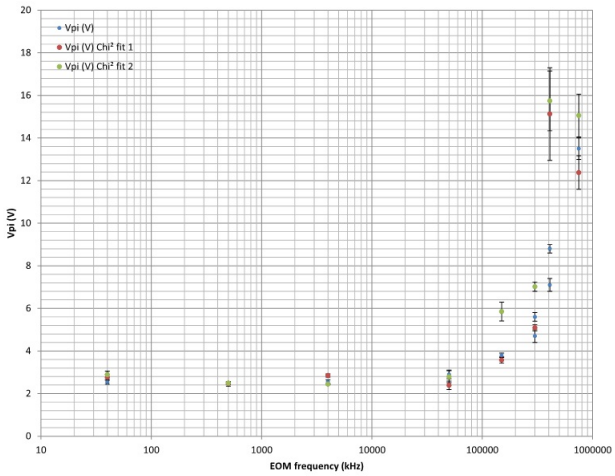

Figure 24: The potential relationship between the frequency at which the EOM is modulated and V_π as found by two different methods. The blue curve follows the method outlined in section 6.3 whereas the second method compared the experimental to the theoretical model using a χ^2 fitting program for each first harmonic peak separately.

One potential source of error in the experimental measurements could be the amplifiers needed to observe the signal from the fast-photodiode on the spectrum analyzer. For frequencies below 200 MHz, a Femto HVA -200M-40-B amplifier was used as it not allow higher frequencies to pass. For the data set this included the frequencies of modulation from 40 kHz to 150 MHz. The amplifier functioned properly for each data set except at 150 MHz where the $\omega+\Omega$ first harmonic peak occurring at 230 MHz was cut in amplitude by the amplifier, resulting in the large difference between the values of V_π found for the two different peaks, as shown by the second fitting method in Figure 24. However, this does not appear to be a problem as the V_π fit to the first harmonic peak at $\omega-\Omega$ occurring at 70 MHz matches the value of V_π fit to the average of the two peaks. The data points taken at frequencies higher than 200 MHz, namely between 300 MHz and 750 MHz, were taken with a Mini-Circuits ZX80-30186-57 amplifier whose frequency range was between 20 MHz and 3 GHz, however, the voltage supply to run the circuit cut frequencies at 1 GHz, limiting the actual frequency range at 1 GHz. This amplifier created more noise than the lower frequency range amplifier, possibly a factor in the increasing values of V_π, however, a smooth curve can be drawn between the points taken with each amplifier, indicating that this does not appear to be a large issue in the varying values of V_π. For the data points taken at 410 MHz it is unknown as to why the two methods of finding V_π result in different values, however, the theoretical model does not fit the experimental data as well at that frequency as it does for other frequencies, as shown in Table 3 f_2 and g_2.

In order to truly test if the use of the two different amplifiers resulted in different values of V_π it would be necessary to take a data set within the range of both amplifiers and compare the resulting values of V_π under the two conditions. If the two amplifiers result in the same value within error, the amplifiers are not the source of problems. There was insufficient time to perform this experiment, thus if this experiment were to be continued taking two data sets at the same frequency with the two different amplifiers would help to confirm or exclude them as a source of error in the measurements.

7. Conclusion

The goal of this experiment was to characterize two fiber optics devices to be used in the laser stabilization project, LASIC II, which is to be used aboard LISA. The two main devices characterized were an Evanescent-Wave Coupler (EWC) and an Electro-Optic Modulator (EOM), while a third device, a non-fibered Acousto-Optic Modulator (AOM), was characterized to be used in an experiment to study the EOM. First the polarization of each devices was studied, in order to determine wether or not they are polarizing maintaining as specified by the manufacturers. This was done by inputting a linearly polarized beam to each of the devices and analyzing the data with Malus' Law, Equation 9, to determine if the resulting output beam was

also linearly polarized. It was found that each of the three devices is indeed polarizing maintaining, where the non-evanescent beam of the EWC has an extinction ratio of 30 dBm, the evanescent beam of the EWC has an extinction ratio of 25 to 33 dBm depending upon the coupling ratio of the beam, the AOM has an extinction ratio of 17.5 dBm and the EOM has an extinction ratio of 30 dBm. Second, the coupling ratio of the EWC was studied, as the device splits an input beam in varying ratios. By changing the position of a micrometer knob on the device and recording the subsequent change in output power of the evanescent beam the device was found to have a mechanical hysteresis. This means that the position of the knob associated with the maximum evanescent beam output depends on how the maximum is found, namely if the position of the knob is increased or decreased. Increasing the knob's position results in a maximum at the position named 1.38 while decreasing the position results in a maximum at the position 1.32. This is not a large issue in the usage of the device as once a maximum is found it is stable, additionally, the manufacturer warns to not rely upon the micrometer to find the maximum evanescent power output. Finally, a heterodyne interferometry experiment was constructed to study the half-wave voltage, V_π, of the EOM by introducing a phase shift to one beam with the EOM and a frequency shift to the second beam with the AOM. Recording the amplitudes of the principle and first harmonic peaks as both the frequency and amplitude of the modulation signal to the EOM were altered allowed the experimental data to be compared to a theoretical model depending upon V_π, where two different fitting methods produced similar values of V_π. It was found that V_π changes with the frequency of modulation, however the exact relationship between the two quantities is unknown and the manufacturer does not warn of this dependence. Also unexpected are the large values of V_π for frequencies over 300 MHz, where V_π exceeds the maximum voltage amplitude that can be applied to the EOM, presenting problems if the device is used in this frequency range, as is planned for the LASIC II experiment. A source of error in these measurements may be the amplifiers used in the experimental apparatus, however this avenue requires further study to be conclusive.

8. Acknowledgements

This research was conducted at the Astroparticule et Cosmologie Laboratory in Paris, France, and was made possible by the University of Florida and the National Science Foundation's Research Experience for Undergraduate Students program. I would like to thank my advisor, Hubert Halloin, for his guidance during this project and everyone at the APC who graciously helped make finicky optical components function properly.

9. Appendix A: All Measurements of Peak Stabilities and V_π for the EOM

This appendix contains all data used to find the relationship between the half-wave voltage, V_π, of the EOM and the frequency at which the device is modulated, excluding the data set at a modulation frequency of 40 kHz which is presented in Section 6.3. The first column presents the peak stability data for each measurement, showing that the principle peak's amplitude is stable and that the amplitudes of the first harmonic peaks follow one another, such that the average of the two peaks can be taken, and is graphed on the same plot. The second column presents the experimental data fit to the theoretical model in order to find the value of V_π which best fits the data. The frequency of each measurement and the value of V_π which fit the data is presented in the title of each graph and the data is compiled for comparison in Figure 24.

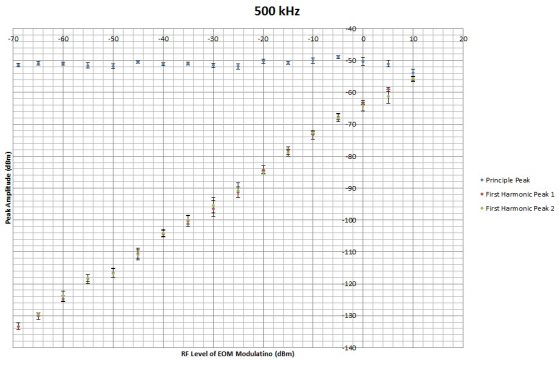

(a_1)

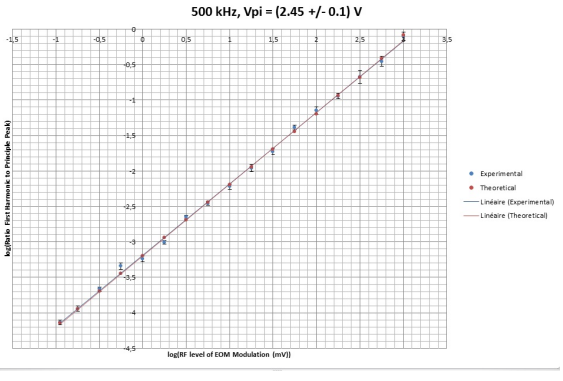

(a_2)

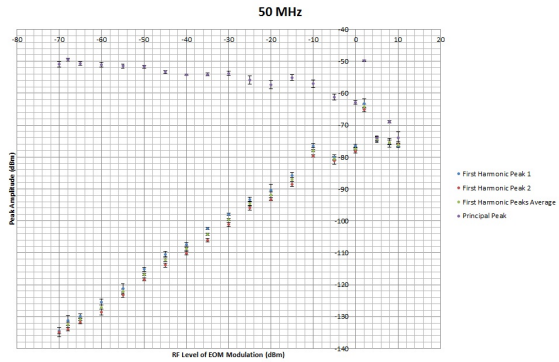

(b_1)

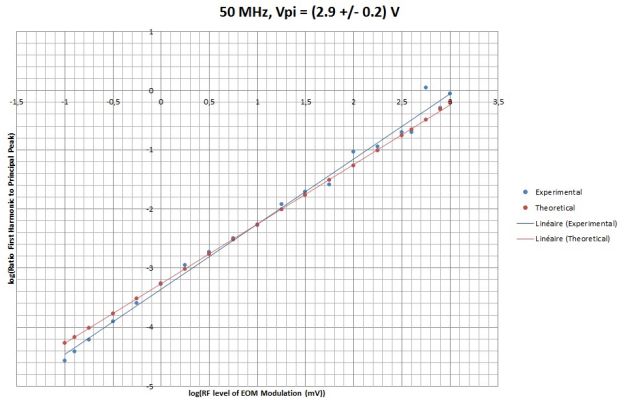

(b_2)

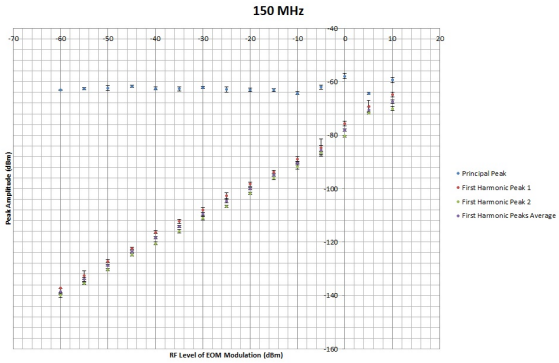

(c_1)

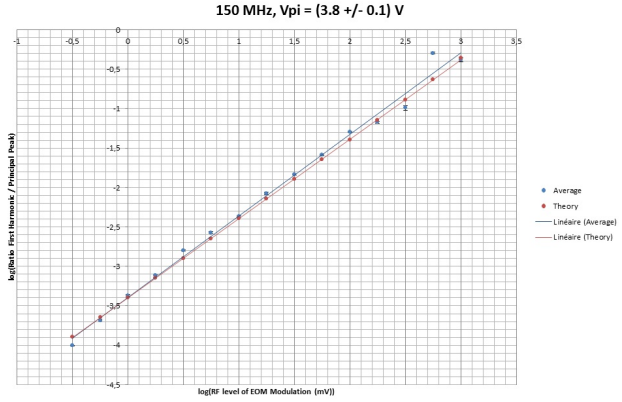

(c_2)

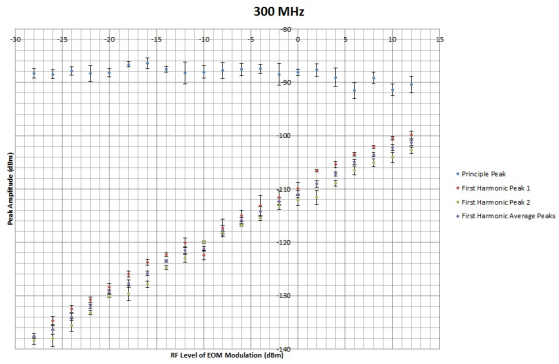

(d_1)

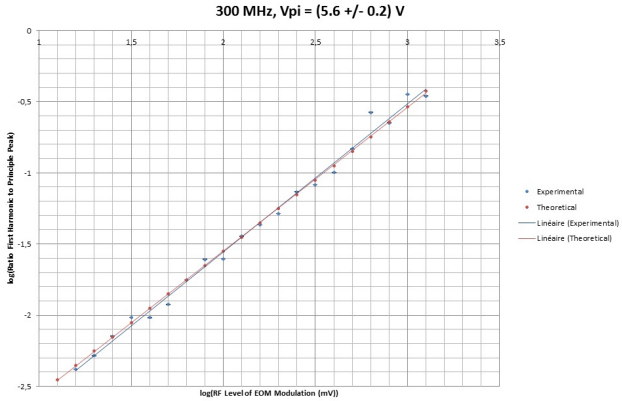

(d_2)

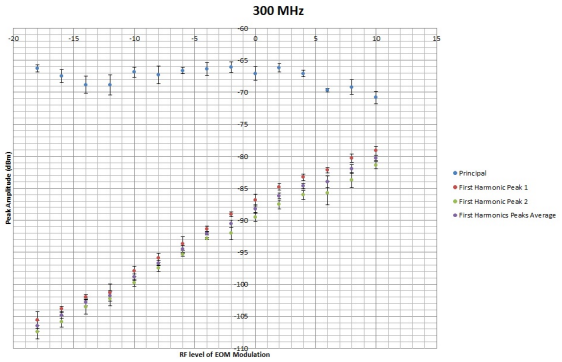

(e_1)

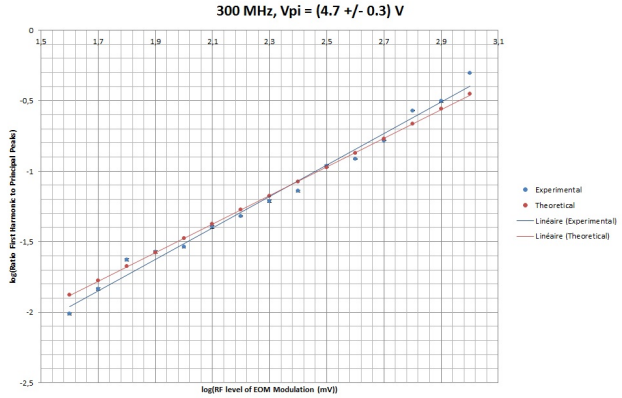

(e_2)

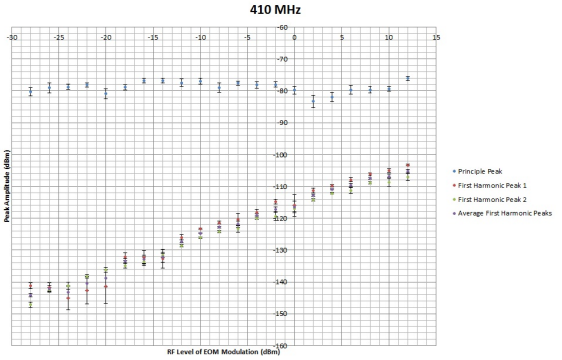

(f_1)

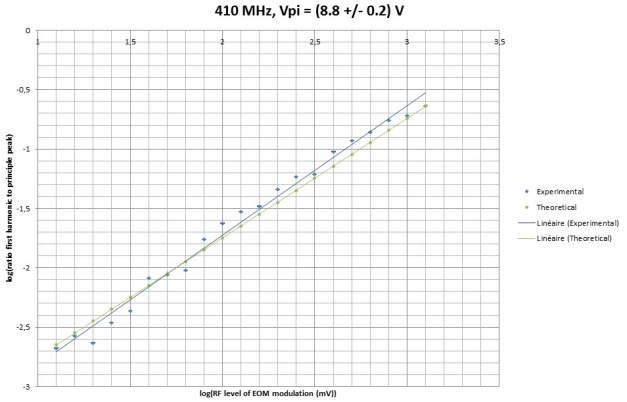

(f_2)

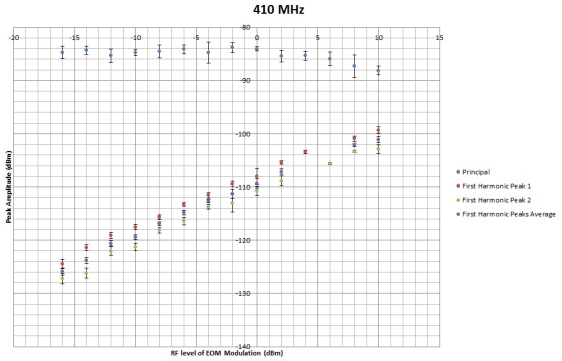

(g_1)

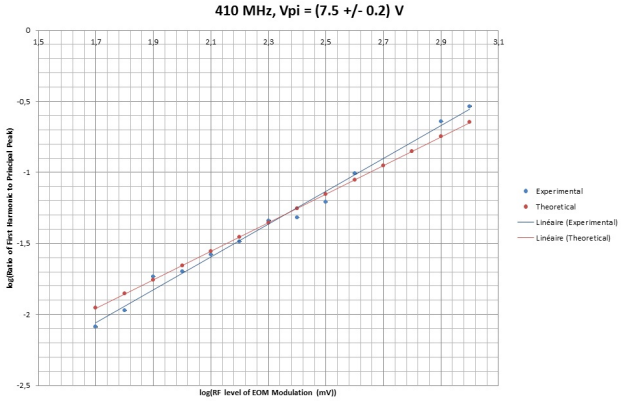

(g_2)

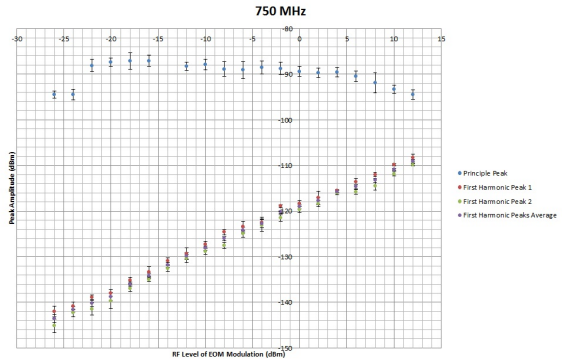

(h_1)

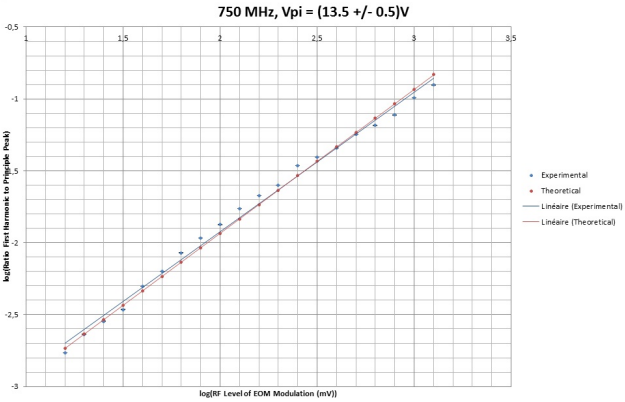

(h_2)

Table 3: The peak stabilities and V_π measurements for the following frequencies, a.) 500 kHz, b.) 50 MHz, c.) 150 MHz, d-e.) 300 MHz, f-g.) 410 MHz, h.) 750 MHz. The data sets for 40 kHz are presented in Section 6.3.

References

[1] Schulz, Bernard. *Gravity From the Ground Up*. Cambridge University Press. 2003.

[2] Maggiore, Michelle. *Gravitational Wave Experiments and Early Universe Cosmology*. 1999.

[3] Argence, B. Halloin. H, et al. *Molecular Laser Stabilization at Low Frequencies for the LISA Mission*. Physical Review D **81**. 2010.

[4] Gondhalekan, Prabhakar. *The Grips of Gravity*. Cambridge University Press. 2001.

[5] Einstein, Albert. Trans. Jeffery, G.B. *On the Electrodynamics of Moving Bodies*. 1905. Trans. 1923.

[6] Einstein, Albert. Trans. Engel, A. *The Foundation of the General Theory of Relativity*. 1916. Trans. 1997.

[7] LIGO Scientific Collaboration & The Virgo Collaboration. *An Upper Limit on the Stochastic Gravitational Wave Background of Cosmological Origin*. Nature **460**. 2009.

[8] NASA. *On the Edge: Gravitational Waves*. `http://imagine.gsfc.nasa.gov/docs/features/topics/gwaves/gwaves.html`. 2003. July 2012.

[9] LIGO. *Introduction to LIGO & Gravitational Waves: Ripples in Space-Time*. `http://www.ligo.org/science/GW-GW2.php`. July 2012.

[10] Argence, Berengere. *Stabilisation de fréquence d'un laser Nd:YAG sur une transition de la molécule de di-iode (I^2) pour la mission spatiale LISA*. 2010.

[11] Giancoli, Douglas. *Physics for Scientists & Engineers with Modern Physics*. 4th Ed. 2008.

[12] Demtröder, Wolfgang. *Laser Spectroscopy: Basic Concepts and INstrumentation*. Springer. 2003.

[13] Halloin, Hubert. et al. *LISA on Table: An Optical Simulator for LISA*. International Conference on Space Optics. 2010.

[14] Pain, H.J. *The Physics of Vibrations and Waves*. John Wiley and Sons. 2005.

[15] Evanescent Optics Inc. *The Wave Guide, Modes and Evanescent Tails Basics*. `http://www.evanescentoptics.com/technical.php?id=37`. August 2012.

[16] Evanescent Optics Inc. *Product Data 905(P)/905(P)-E*. `http://www.evanescentoptics.com/products.php?id=25`. August 2012.

[17] Pinson, Lewis I. *Electro-Optics*. John Wiley and Sons. 1985.

[18] A.A. Opto-Electronic. *Modulators & Fixed - Frequency Shifters*. `http://opto.braggcell.com/index.php?MAIN_ID=101`. August 2012.

[19] Jenoptik Optical Systems, Inc. *Integrated Optical Amplitude and Phase Light Modulators*. `http://www.jenoptik-inc.com/jenoptik-light-modulators/237-integrated-optical-amplitude-and-phase-light-modulators.html`. August 2012.

[20] Klein, Miles V. *Optics*. John Wiley & Sons Inc. 1970.